Neuropsychopharmacology (2010) 35, 641–655

www.neuropsychopharmacology.org

FosB Null Mutant Mice Show Enhanced Methamphetamine Neurotoxicity: Potential Involvement of FosB in Intracellular Feedback Signaling and Astroglial Function

Kumi O Kuroda*[,1], Veravej G Ornthanalai[2], Tadafumi Kato[3] and Niall P Murphy[2,4]

[1]Unit for Affiliative Social Behavior, RIKEN Brain Science Institute, Saitama, Japan; [2]Neuropathology Research Group, RIKEN Brain Science Institute, Saitama, Japan; [3]Laboratory for Molecular Dynamics of Mental Disorder, RIKEN Brain Science Institute, Saitama, Japan

Previous studies show that (1) two members of fos family transcription factors, c-Fos and FosB, are induced in frontal brain regions by methamphetamine; (2) null mutation of *c-Fos* exacerbates methamphetamine-induced neurotoxicity; and (3) null mutation of *FosB* enhances behavioral responses to cocaine. Here we sought a role of FosB in responses to methamphetamine by studying *FosB* null mutant (−/−) mice. After a 10 mg/kg methamphetamine injection, *FosB*(−/−) mice were more prone to self-injury. Concomitantly, the intracellular feedback regulators of *Sprouty* and *Rad-Gem-Kir* (RGK) family transcripts had lower expression profiles in the frontoparietal cortex and striatum of the *FosB*(−/−) mice. Three days after administration of four 10 mg/kg methamphetamine injections, the frontoparietal cortex and striatum of *FosB*(−/−) mice contained more degenerated neurons as determined by Fluoro-Jade B staining. The abundance of the small neutral amino acids, serine, alanine, and glycine, was lower and/or was poorly induced after methamphetamine administration in the frontoparietal cortex and striatum of *FosB*(−/−) mice. In addition, methamphetamine-treated *FosB*(−/−) frontoparietal and piriform cortices showed more extravasation of immunoglobulin, which is indicative of blood–brain barrier dysfunction. Methamphetamine-induced hyperthermia, brain dopamine content, and loss of tyrosine hydroxylase immunoreactivity in the striatum, however, were not different between genotypes. These data indicate that FosB is involved in thermoregulation-independent protective functions against methamphetamine neurotoxicity in postsynaptic neurons. Our findings suggest two possible mechanisms of FosB-mediated neuroprotection: one is induction of negative feedback regulation within postsynaptic neurons through *Sprouty* and *RGK*. Another is supporting astroglial function such as maintenance of the blood–brain barrier, and metabolism of serine and glycine, which are important glial modulators of nerve cells.
Neuropsychopharmacology (2010) **35,** 641–655; doi:10.1038/npp.2009.169; published online 4 November 2009

Keywords: FosB; methamphetamine; neurotoxicity; astroglia; sprouty; Rad-Gem-Kir (RGK) family

INTRODUCTION

Amphetamines, substituted amphetamines (such as methamphetamine (METH), and 3,4-methylenedioxymethamphetamine (MDMA or 'ecstasy')) and cocaine are widely abused psychostimulants (Sulzer *et al*, 2005). Whereas cocaine blocks the activity of dopamine, norepinephrine, and serotonin transporters, most amphetamine derivatives promote the release of these biogenic amines by reverse transport, effectively discharging enormous amounts of biogenic amines into the extracellular space. Regardless of the mechanism, a major outcome is a strong potentiation of biogenic amine signaling, and it is this effect that is widely believed to underlie the abuse potential of these drugs. Repeated administration of lower doses or a single high-dose administration of amphetamines may lead to depletion of dopamine and serotonin by causing degeneration of neuronal terminals (Krasnova and Cadet, 2009). Such terminal degeneration is not only long-lasting but also recoverable in rodents, as these monoaminergic neurons themselves are resistant (Bowyer and Schmued, 2006b). In contrast, amphetamines can elicit death of neurons post-synaptic to these monoaminergic terminals in many forebrain regions such as the striatum and the frontal and somatosensory cortices (Krasnova and Cadet, 2009). Two forms of cell death have been implicated in this process (Davidson *et al*, 2001; Gold *et al*, 2009). One is apoptotic cell death, also referred to as programmed cell death, which is characterized by cell shrinkage, specific DNA fragmentation

*Correspondence: Dr KO Kuroda, Unit for Affiliative Social Behavior, E-mail: oyako@brain.riken.jp

[4]Current address: Department of Psychiatry and Biobehavioral Sciences, Semel Institute for Neuroscience and Human Behavior, University of California at Los Angeles, Los Angeles, CA, USA.
Received 12 March 2009; revised 17 August 2009; accepted 3 September 2009

at about 180 bp intervals, and activation of cysteine proteases called caspases. The other form of cell death, necrosis, is a very rapid process, associated with cell swelling, spillage of intracellular substances into surrounding tissue, and nonspecific DNA damage.

Multiple events, including oxidative stress, excitotoxicity (toxicity caused by glutamate release), hyperthermia, mitochondrial and endoplasmic reticulum stress, and the blood–brain barrier (BBB) dysfunction, are implicated in amphetamine-induced neurotoxic effects (Krasnova and Cadet, 2009). These events appear to be intimately related. For example, preventing hyperthermia by cooling the ambient temperature to 4°C can decrease molecular markers of oxidative stress, attenuate dopaminergic and serotonergic terminal depletion, and decrease neuronal death in the parietal cortex (Bowyer, 1995; Eisch *et al*, 1998). Similarly, the glutamate receptor antagonist MK-801 can attenuate hyperthermia, dopaminergic and serotonergic terminal degeneration, and neuronal death in the parietal cortex (Eisch *et al*, 1998; Tata and Yamamoto, 2007). As such, it is still unclear which mechanism is the most upstream and/or responsible for each neurotoxic end point. Interestingly, however, a dopamine transport inhibitor administered before METH can only prevent striatal tyrosine hydroxylase immunoreactivity loss, but not hyperthermia or neuronal death in the parietal cortex (Eisch *et al*, 1998). In addition, it has been shown that the striatal subregion that contains the greatest number of degenerated neurons is different from the subregion showing greatest loss of tyrosine hydroxylase immunoreactivity (Bowyer *et al*, 2008). It is therefore likely that mechanisms of striatal dopamine terminal damage exist independent of the mechanisms responsible for postsynaptic cell injury and hyperthermia.

Amphetamines stimulate the expression of many immediate early genes, particularly those of the Fos family transcription factors, which include c-Fos, FosB, Fra-1, and Fra-2 (Herdegen and Leah, 1998). ΔFosB, a truncated splice variant of FosB, is induced in the striatum by chronic exposure to abused drugs (Nestler, 2001). The persistent expression of ΔFosB has been implicated in long-term adaptations that underlie patterns of behavior characteristic of addiction. Previous studies have also shown that *FosB* null mutant (−/−) mice show exaggerated locomotor activation following initial cocaine exposure and robust conditioned place preference to a lower dose of cocaine (Hiroi *et al*, 1998). In addition, c-*Fos*(−/−) and (+/−) mice show exacerbated METH-induced neurotoxicity as reflected in a greater loss of striatal tyrosine hydroxylase-like immunoreactivity and dopamine-reuptake sites and more neuronal apoptosis in their cortices and striata. These results suggest that Fos family proteins may be involved in the protective mechanisms against METH-induced neurotoxicity.

Being important elements of transcriptional regulation of cellular functions, c-Fos and FosB are also likely to be involved in the regulation of many behaviors. An example is parental behavior, which arises from neuronal activity in the medial preoptic area of the hypothalamus (Brown *et al*, 1996; Numan *et al*, 1998). As to this, *FosB*(−/−) mice show abnormal parenting (Brown *et al*, 1996). Our previous studies suggest that the role of *FosB* in this behavior is to induce in downstream target genes such as Sprouty1 (*SPRY1*) and *RAD*, under the control of extracellular signal-regulated kinase (ERK) (Kuroda *et al*, 2007). The Sprouty family consists of three members in mouse, SPRY1, SPRY2 and SPRY4, and represents a major class of ligand-inducible inhibitors of the receptor tyrosine kinase (RTK)-dependent ERK signaling pathway (Mason *et al*, 2006). RAD is a member of the *Rad-Gem-Kir* (RGK) family small GTP-binding proteins that encompasses RAD, GEM/KIR, REM and REM2, which function as potent inhibitors of voltage-dependent calcium channels (Kelly, 2005). The ERK–FosB–SPRY1/RAD signaling therefore appears to provide critical feedback regulation of neuronal adaptation in the initiation of parental care (Kuroda *et al*, 2007). It seems likely that this intracellular signaling cascade is also involved in other behaviors, such as those in response to METH and other psychostimulants. For instance, *c-Fos* heterozygous mutant (+/−) mice, in which METH-induced dopaminergic terminal damage and neuronal apoptosis are exacerbated (Deng *et al*, 1999), show significant impairment in *GEM* (a member of RGK family) upregulation in the striatum compared with wild-type mice on METH administration (Cadet *et al*, 2002). Administration of MDMA causes ERK activation and subsequent upregulation of *REM2*, another member of RGK, along with *c-Fos* and *FosB* in the striatum (Salzmann *et al*, 2006). Induction of *FosB* and *REM2*, but not *c-Fos* by MDMA is blocked by SL327, a specific inhibitor of ERK phosphorylation (Salzmann *et al*, 2006).

The purpose of this study was to identify the role of FosB in response to METH. Our working hypothesis was that the ERK/calcium-c-Fos/FosB-Sprouty/RGK intracellular signaling acts as a general negative feedback loop for ERK activation and calcium influx in stimulated neurons. If this is true for METH-activated neurons, the *FosB*(−/−) mice would show enhanced cellular, neurochemical, and behavioral responses to METH, and decreased Sprouty/RGK expression profiles. We found that *FosB*(−/−) mice indeed showed greater neuronal degeneration in cortices and the striatum, increased incidence of self-injuries, altered regulation of intracellular *Sprouty* and *RGK* family transcripts compared with those of their wild-type littermates. In addition, *FosB*(−/−) mice showed signs of astroglial dysfunction, reflected as perturbed regulation in brain amino-acid contents and METH-induced BBB disruption.

MATERIALS AND METHODS

Animals

All animal experiments were approved by the animal experiment committee of RIKEN. Wild-type C57BL/6J mice were purchased from Japan SLC (Hamamatsu, Japan). The *FosB*(−/−) mouse strain was obtained from the Jackson Laboratory (strain C; 129S-*Fosb*^{tm1Meg}/J). All of the mice were backcrossed at least five times to C57BL/6J and generated by *FosB*(+/−) intercrosses. Mice were housed in ventilated shoebox cages (267 × 483 × 152 mm) with access to food and water *ad libitum* and were maintained under a 12 : 12 h light/dark cycle. TEK-Fresh Standard (Harlan, Madison, WI, USA) bedding was used for animal housing. All mice used in this study were adult males of 10–20 weeks of age, and studies included age-matched controls. Four

separate groups of *FosB*(−/−) and (+/+) mice were used in the following four major sets of studies: (1) histological studies, (2) hyperthermia, (3) gene expression, and (4) locomotor activity/analysis of brain biogenic amine and amino-acid content. The effects of METH on self-injury were observed across studies except in experiment 4. Mice were single-housed in clean cages at least 1 day before METH administration, except in experiment 4, where mice remained group-housed throughout.

Overview of METH Treatment Regimens Used

For histological studies of METH-induced neuronal damage, we gave mice four injections of 10 mg/kg METH (methamphetamine hydrochloride, uncorrected for molecular salt and water content; Dainippon Pharmaceuticals, Tokyo, Japan) at 2-h intervals or saline vehicle subcutaneously (10 ml/kg). These mice were transcardially perfused 3 days later, as previous reports suggest that this time point is where peak neuronal degeneration is observed (Eisch *et al*, 1998). Mice studied for the hyperthermic effects of METH were administered the same regimen as the histological studies. For the gene expression study, mice were given a single 10 mg/kg injection of METH and killed by cervical dislocation 2 h later, as changes in FosB protein levels and gene expression have been reported to peak about 2 h after METH stimulation (Cadet *et al*, 2002; Hiroi *et al*, 1997). For locomotor activity and analysis of brain biogenic amine and amino-acid content, mice were first administered a 1.5 mg/kg dose of METH. On the following day, the mice were administered 10 mg/kg METH four times every 2 h. After 2 days, the mice were administered another 1.5 mg/kg METH. More detailed descriptions of the treatment regimens and rationales are provided in the appropriate sections below.

Temperature Measurement

Core body temperature was recorded using a Bat-10 thermometer equipped with a RET-3 mouse rectal probe (Physitemp Inc., Clinton, NJ, USA). It has been reported that c-*Fos*(−/−) mice are more susceptible to rectal injury and are more prone to fatality by repeated rectal temperature measurements in conjugation with METH administration (Deng *et al*, 1999). Nonetheless, *FosB*(−/−) mice were not significantly susceptible to this protocol compared to *FosB*(+/+) mice (data not shown).

Behavior and Self-Injury After METH Administration

At 30 min following the first 10 mg/kg METH injection, we briefly observed the subject mice from outside the cage. All of the mice showed at least one of the following behaviors: stereotypic sniffing, vigorous chewing, increased locomotor activity, head-bobbing, and excessive salivation, as previously described (Eisch *et al*, 1998; Wagner *et al*, 2004). These observations were subjective and qualitative, but not quantitative, as the purpose of the observation was to confirm the proper METH injection. At 2 h after the injection, we carefully sought evidence of bleeding on the bedding. Whenever signs of bleeding were observed, mice were further examined to identify skin lesions. We repeated this survey just before each subsequent injection to seek for self-injury inflicted after the previous injection. Right after each injection, we confirmed that there was no immediate blood leakage from the injection site itself. A single mouse that showed immediate bleeding from the injection site was excluded from the experiment. Throughout this study, we did not observe any major convulsions in either genotype, though our rudimentary observation scheme may have been insufficient to detect minor convulsions.

Histological Analyses

At 3 days after the four injections of 10 mg/kg METH at 2-h intervals, we anesthetized and perfused mice with 4% paraformaldehyde in sodium phosphate-buffered saline at pH 7.4. Brains were postfixed and cryosectioned at 40 μm. Every fifth serial coronal section was used for tyrosine hydroxylase immunostaining, mouse IgG immunostaining, Fluoro-Jade B (FJB) staining, TdT-mediated dUTP-biotin nick-end labeling (TUNEL) method, or cleaved caspase-3 immunodetection. Although the TUNEL method is a widely used and well-established assay to detect apoptotic cells by labeling double-stranded DNA fragmentation, immunodetection of cleaved caspase-3 is more specific and sensitive to apoptotic cells (Gown and Willingham, 2002). FJB is a fluorescent dye that has a high affinity for degenerating neurons, regardless of the specific insult or mechanism of cell death (Schmued and Hopkins, 2000).

Indirect immunohistochemical analyses of free-floating brain sections were performed essentially as described (Berghorn *et al*, 1994; Kuroda *et al*, 2008). Briefly, brain sections were incubated overnight with a primary antibody and then incubated with the appropriate biotin-conjugated secondary antibody (Vector, Burlingame, CA, USA). The signal was intensified and visualized using a Vectastain Elite ABC kit and a diaminobenzidine substrate kit (Vector). Sections were mounted on gelatin-coated slides. Bright-field images were acquired using a digital camera DXM1200C and an Eclipse 80i microscope (Nikon, Kawasaki, Japan). The primary antibodies used in this study were an anti-tyrosine hydroxylase mouse monoclonal antibody (1 : 18 000, MAB318; Chemicon, Temecula, CA, USA) and an anti-cleaved caspase-3 rabbit polyclonal antibody (1 : 500, ASP175; Cell Signaling, Danvers, MA, USA; data not shown).

To measure the relative intensity of tyrosine hydroxylase immunoreactivity, we used bright-field images of 4–6 brain sections between anterior-posterior positions (AP) +1.5 to +0.8 mm relative to bregma (Franklin and Paxinos, 2007). Rectangular areas of the images of tyrosine hydroxylase immunostaining in the dorsal striatum (randomly taken from the caudate putamen) and the ventral striatum (taken from the nucleus accumbens core) from each photomicrograph were collected. The size of the rectangular field was varied to cover the maximum amount of the anatomical region of interest, but not any adjacent areas. The optical density (arbitrary units) of these areas was quantified using Scion Image software version 4.0.3 (Scion Corporation, Frederick, MD, USA) by an experimenter blind to the experimental groups. The optical density of immunostaining in the corpus callosum was subtracted as background. The relative density of the dorsal or ventral striatum was

then averaged in each animal and subjected to statistical analysis.

Evaluation of BBB integrity using IgG immunoreactivity was performed essentially as described (Bowyer and Ali, 2006a; Bowyer *et al*, 2008). Briefly, the same staining protocol as the tyrosine hydroxylase immunostaining was applied, except that sections were directly incubated with a biotin-conjugated anti-mouse IgG secondary antibody (1 : 2000; Vector) after the blocking step. We confirmed the previous finding that IgG immunoreactivity in the cortex and striatum after neurotoxic METH treatment was confined to perivascular tissue and weakly in microglial cells (Bowyer *et al*, 2008). To quantify the extent of IgG extravasation, we used bright-field images of 8–10 brain sections between AP +1.2 to −0.7 mm. The numbers of discrete cross-sections of blood vessels surrounded by IgG immunostaining were manually counted. We attempted to omit microglia-like IgG-positive cells from the counts, though some minor ambiguities may have been introduced. As a precaution, we therefore designated these as 'IgG immunoreactive bodies' according to a previous study (Bowyer and Ali, 2006a). The density of IgG immunoreactive bodies was averaged in each brain area of individual animals and subjected to statistical analysis.

Detection of degenerating neurons by FJB staining was performed essentially as described (Schmued and Hopkins, 2000). Briefly, the adjacent serial sections used for IgG immunohistochemistry were mounted on gelatin-coated slides and dried at room temperature. Slides were washed with distilled water for 10 min, gently shaken in 0.06% potassium permanganate for 15 min, and washed in distilled water again for 1 min. Slides were then gently shaken in 0.0005% FJB (Histo-Chem Inc., Jefferson, AR, USA) and 0.1% acetic acid solution for 30 min in the dark, washed in distilled water, and air-dried in the dark. The slides were dehydrated and coverslipped, and observed as described above, except fluorescent microscopy was applied. The same anatomical areas were observed as in the IgG staining described above. As previously shown, FJB stains the cell bodies, dendrites, axons and axon terminals of degenerating neurons but does not stain healthy neurons, myelin, vascular elements, or neuropil (Schmued and Bowyer, 1997; Schmued and Hopkins, 2000). In addition, it is known that relatively small morphological differences exist between healthy and degenerating neurons. We therefore identified individual FJB-positive neuronal cell bodies by neuronal morphology and counted them manually using the acquired images of each brain area. The density of FJB-positive neurons was averaged in each brain area of individual animals and subjected to statistical analysis.

Quantitative Real-Time PCR (qRT-PCR) Detection of mRNA

Brain tissue dissections were performed essentially as described (Glowinski and Iversen, 1966) using a mouse brain atlas (Franklin and Paxinos, 2007). Briefly, animals were killed by cervical dislocation and decapitated. After the skin on the skull was removed, the head was chilled in ice-cold saline for 2 min. After the skull was removed, 1 mm parasagittal cuts starting from AP +2 mm (relative to bregma) toward the posterior were carried out on both hemispheres using a scalpel. Then AP +2 and +3 mm coronal cuts were carried out, and the resultant coronal section was placed on saline-soaked filter paper on ice. After removing tissue ventral to the rhinal fissure, the resultant rostral-most cerebral cortical tissue (designated as 'frontoparietal cortex' in this study for simplicity) was collected into 2 ml tubes containing 1.2 ml Trizol reagent (Invitrogen, Carlsbad, CA, USA) on ice. The tissue was homogenized immediately by passing through a 20-gauge needle 20 times and then through a 26-gauge needle 10 times using a 1 ml syringe. For striatal tissue preparation, the lateral hemispheres separated by the parasagittal cuts were soaked in ice-cold saline for 2 min. The striatum was then separated from the cortex by inserting a spatula into the border between the striatum and the external capsule from anterior to posterior using a scooping motion. Finally, the tissue ventral to the anterior commissure was removed, and the resultant bilateral tissue (designated as 'striatum' in this study) was collected and homogenized in Trizol in the same manner as the frontoparietal cortex. To minimize the duration from the animal decapitation to complete tissue homogenization, three experimenters performed this procedure.

Total RNA from the striatum and the frontoparietal cortex was isolated using Trizol and further purified by RNeasy Micro kit (Qiagen, Hilden, Germany). qRT-PCRs were performed with an ABI Prism 7000 Sequence Detector Systems (Applied Biosystems, Foster City, CA, USA) as previously described (Kuroda *et al*, 2007). The relative amount of specific mRNA was calculated as $2^{(Ct(\text{each gene})-Ct(GAPDH))}$ in triplicate. The average C_t (*GAPDH*) did not differ between groups (data not shown). The *Taq*Man probe IDs unique to this study were Mm00494584_m1 (*GEM*), Mm 00600529_m1 (*REM2*), Mm 00442344_m1 (*SPRY2*), and Mm 00442345_01 (*SPRY4*).

Locomotor Assays

To determine the effect of the neurotoxic schedule of METH administration on the psychomotor effects of a low (1.5 mg/kg) dose METH administration, we administered to a cohort of mice the same neurotoxic regimen of METH described above, preceded and followed by low-dose administrations of METH, during which locomotion was measured. Thus, all animals were group-housed before and throughout this part of the study except for during locomotor monitoring. On the first day, all mice were given a single subcutaneous injection of 1.5 mg/kg METH or saline before being individually placed in a 25 × 25 × 38.5 cm locomotor-monitoring apparatus (Truscan, Coulbourn Instruments, Allentown, PA) for 45 min. The following day, mice were given four serial injections of 10 mg/kg METH or saline at 2-h intervals in the home cage. Mice were undisturbed on day 3. On the fourth day, all mice were administered 1.5 mg/kg METH or saline, and locomotion was monitored for 45 min.

Biochemical Analyses of Tissue Biogenic Amine and Amino-Acid Contents

To investigate the effect of the neurotoxic schedule of METH administration on central biogenic amine systems,

the same cohorts of mice used in the locomotor assay study were killed immediately following the locomotor-monitoring session on the fourth day by decapitation. The brains were rapidly removed and frozen on crushed dry ice before storage at −80°C. This strategy was chosen to minimize the number of animals required for the overall study, even though this strategy led to the caveat that the results from this part of the study were not directly comparable with the hyperthermia, immunoreactivity, and FJB studies described above, as they received marginally higher (7.5% more in terms of quantity) exposure to METH.

Coronal sections (150 μm) were prepared on a cryostat and mounted immediately onto gelatinized slides. Using a 1 mm diameter biopsy punch (Kai Medical, Gifu Prefecture, Japan), we took circular tissue punches from the frontoparietal cortex, dorsal, and ventral striatum. A total of 5, 12, and 10 punches were pooled by region from the frontoparietal cortex (AP coordinates 5.90–5.34 mm interaurally, according to the atlas (Franklin and Paxinos, 2007)), dorsal striatum (4.90–3.82 mm) and ventral striatum (5.14–4.18 mm), respectively of individual mice. Samples were immediately stored at −80°C until further analysis.

The biochemical contents of the tissue were assayed as previously described (Katayama *et al*, 2008) by high-pressure liquid chromatography (HPLC) coupled to either electrochemical detection (for biogenic amines) or fluorometric detection following derivatization with *o*-phthaldehyde (for amino acids). Briefly, extracts from the tissue punches were obtained by sonication at 4°C in 60 μl of extraction buffer for the frontoparietal cortex or 100 μl for the dorsal and ventral striatum. The extraction buffer consisted of perchloric acid (0.1 M) and isoproterenol (200 nM) or L-norleucine (200 μM) as internal standards for monoamine and amino-acid analyses, respectively. The amino-acid standards used were composed of the L-type stereoisomers (H-type standard; Wako Pure Chemicals, Japan with additional L-type amino acids and γ-aminobutyric acid (GABA) standards incorporated). A commercial protein assay kit (Bio-Rad, Hercules, CA) was used to determine the protein content of the extracts. Turnover rates were calculated as follows: DA turnover rate = (DOPAC) + (HVA)/(DA); 5-HT turnover rate = (5-HIAA)/(5-HT).

Statistical Analyses

For the statistical analysis of the data, various analyses of variance (ANOVAs) and Fisher's exact probability tests were applied where appropriate (see Results section). Significance levels were set at $p<0.05$ (two tailed). Statistical analyses were performed using SPSS 10.0 for Windows (SPSS Japan, Tokyo, Japan) or StatView (StatView, Berkley, CA). All data are expressed as mean ± standard error of the mean (SEM).

RESULTS

Enhanced METH Neurotoxicity in *FosB*(−/−) Mice

To test whether *FosB*(−/−) neurons exhibit enhanced vulnerability to METH-induced excitotoxicity, we used a neurotoxic regimen of four injections of 10 mg/kg METH spaced at 2-h intervals as previously described (Eisch *et al*, 1998; Deng *et al*, 1999; Kita *et al*, 2003). *FosB*(+/+) and (−/−) mice were killed 3 days later and examined for neurodegeneration by FJB labeling. FJB is a fluorescent dye that has high affinity for degenerating neurons, regardless of specific insult or mechanism of cell death (Schmued and Hopkins, 2000). Consistent with previous reports (Ryan *et al*, 1990; Schmued and Bowyer, 1997; Deng *et al*, 2001), neurodegeneration occurred in the frontoparietal and piriform cortices and in the striatum (Figure 1a), in METH-treated both *FosB*(+/+) and (−/−) mice. We found some FJB-positive neurons in the hippocampal complex as well, but to a much lesser extent (data not shown). In both *FosB*(+/+) and (−/−) saline-treated animals, FJB-positive neurons were rarely found in any brain area (Figure 1b).

The densities of FJB-positive degenerating neurons were quantified and analyzed by a two-way ANOVA with intersubject factors of genotype and treatment (Figure 1b). Significant effects of treatment were found in the frontoparietal cortex ($F_{1,18}=24.84$, $p<0.001$), striatum ($F_{1,18}=5.00$, $p=0.038$), and piriform cortex ($F_{1,18}=8.40$, $p=0.010$). Significant effects of genotype were found in the frontoparietal cortex ($F_{1,18}=15.32$, $p=0.001$) and striatum ($F_{1,18}=4.61$, $p=0.046$), but not in the piriform cortex ($F_{1,18}=2.06$, $p=0.169$). Significant genotype–treatment interactions were found in the frontoparietal cortex ($F_{1,18}=15.37$, $p=0.001$) and striatum ($F_{1,18}=4.59$, $p=0.046$), but not in the piriform cortex ($F_{1,18}=2.07$, $p=0.168$). After METH treatment, therefore, the frontoparietal cortex and striatum of *FosB*(−/−) mice contained significantly more FJB-positive neurons than those of their *FosB*(+/+) littermates. In contrast, we did not find a significant genotype–treatment interaction in the piriform cortex, possibly because there was large individual variability in the number of degenerating neurons in both (−/−) and (+/+) mice. These data suggested that FosB protects neurons in the frontoparietal cortex and striatum from METH-induced neurotoxicity.

FJB-positive cells tended to cluster in subregions. In the parietal cortex, most of the degenerating cells were layer-III pyramidal neurons and superficial layer-IV multipolar neurons in the parietal cortex area 1, as previously described (Eisch *et al*, 1998). Moreover, FJB-positive cells tended to be found in the very center of the striatum. In the piriform cortex, the FJB-positive cells were clustered in the dorsal endopiriform area. These distribution patterns of FJB-positive neurons are the same in both genotypes. Notably, these distribution patterns were very similar to the area of BBB dysfunction identified and described below.

We also sought evidence of differences in the amount of apoptosis by means of the TUNEL histochemical method and anticleaved caspase-3 immunodetection method. We observed much smaller numbers of apoptotic neurons by either anticleaved caspase-3 immunoreactivity or the TUNEL method in forebrain regions 3 days after four 10 mg/kg injections in both *FosB*(−/−) and (+/+) mice compared with the numbers of FJB-positive neurons (data not shown). Thus, under our experimental conditions, it appeared that METH-induced neuronal death in *FosB*(−/−) mice was largely due to necrosis or some other nonapoptotic regulated death program.

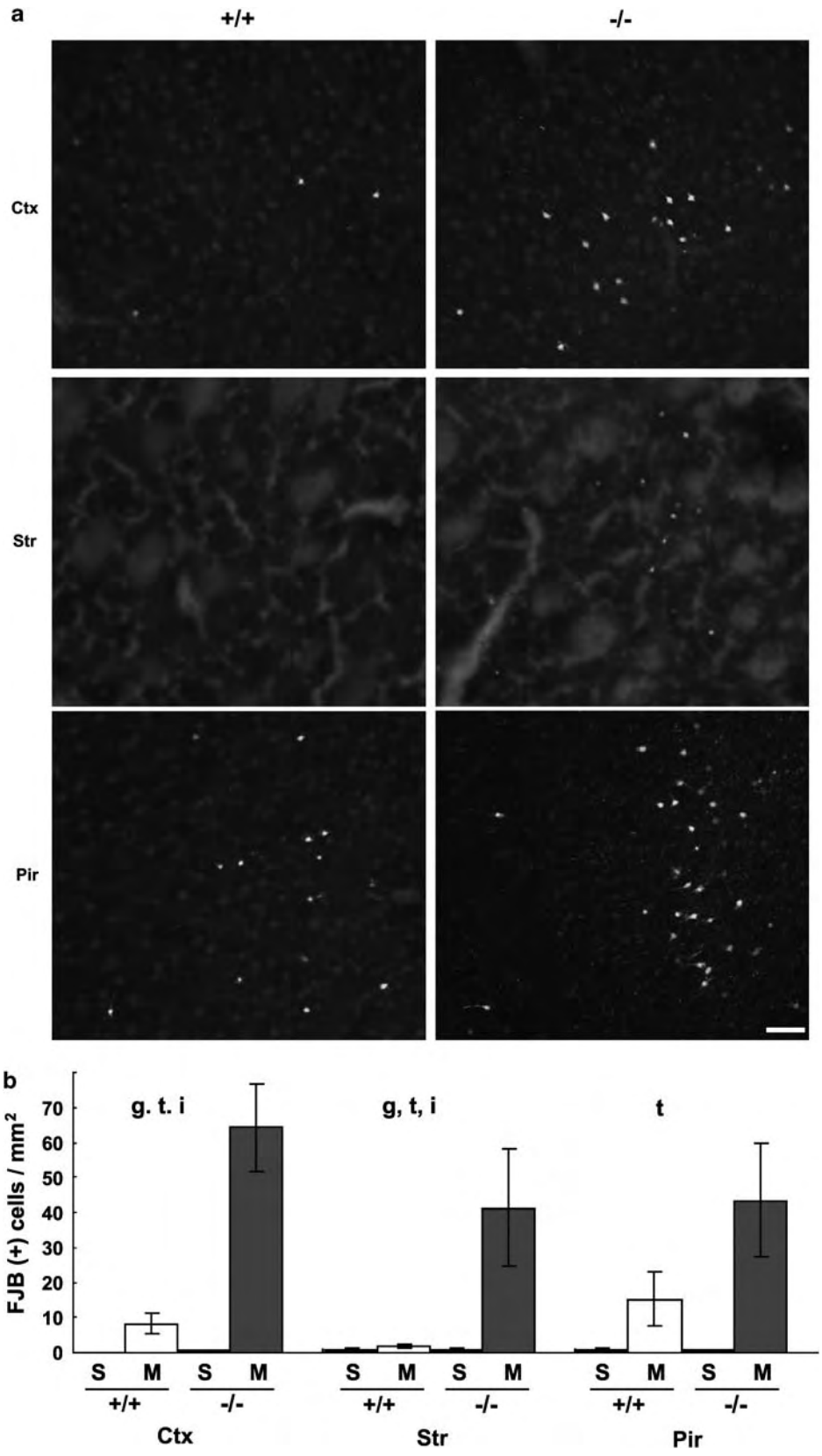

Figure 1 Effects of the *FosB* mutation on neurodegeneration after neurotoxic methamphetamine (METH) administration. *FosB*(+/+) and (−/−) mice were treated with four injections of saline (S, $n=5$ each) or 10 mg/kg METH (M, $n=6$ each) and were examined for neurodegeneration 3 days later by Fluoro-Jade B (FJB) staining. (a) Fluorescent microscopy of fields from the parietal cortex (Ctx), the striatum (Str), and the piriform cortex (Pir) of METH-treated mice. These areas were taken from the rectangular areas shown in Figure 7a. Scale bar = 100 μm. (b) Mean ± SEM density of FJB-positive degenerating cells in each area. Letters above the bars indicate significant effects ($p<0.05$) of genotype (g), treatment (t), and/or genotype–treatment interaction (i) by a two-way analysis of variance (ANOVA) with the intersubject factors of genotype and treatment.

No Differences in METH-Induced Hyperthermia in *FosB*(−/−) Mice

Methamphetamine-induced neurodegeneration is mediated at least partly by hyperthermia (Bowyer, 1995). Thus, we examined the core body temperature of *FosB*(−/−) and (+/+) mice during the neurotoxic regimen of METH administration. Using a repeated-measures ANOVA with the intersubject factors of genotype and the within-subject factor of time point, we found a significant effect of time in core body temperature ($F_{10,80} = 28.27$, $p < 0.001$) due to a progressive increase in body temperature in both genotypes, which returned to basal levels by the end of the 7-h recording period (Figure 2). No significant effects of genotype were found in core body temperature after METH injection ($F_{1,8} = 0.047$, $p = 0.834$). *FosB*(−/−) mice therefore did not show altered susceptibility to METH-induced hyperthermia, thus eliminating this factor as the primary cause of enhanced neurodegeneration in these mice.

Increased Incidence of Self-Injury in METH-Treated *FosB*(−/−) Mice

It has been reported that high doses of METH induce self-injurious behaviors in mice, defined as self-biting and scratching that causes breaks in the skin (Kita *et al*, 2003). We observed signs of bleeding on the cage bedding of some *FosB*(−/−) mice after the first 10 mg/kg METH injection. Five out of eight bleeding (−/−) mice exhibited clear skin lesions (Table 1), mostly with obvious marks of insults by teeth or nails. These skin lesions were attributed to self-inflicted biting and scratching, as mice were single-housed throughout these experiments. It was highly unlikely that these lesions were caused just by falling on or hitting the cage wall, the wire lid, water valve, or ventilation nozzle. The locations of the lesions did not show any relationship with the site of METH injection. In the most severe case, an *FosB*(−/−) mouse had 0.5 × 1 cm detachment of skin from its chest and the ventral part of the neck, and the underlying musculature was exposed. For the remaining three bleeding mice, we were unable to identify any obvious skin lesion, though smaller injuries to the tongue or oral cavity due to oral dyskinesia could have possibly occurred (Wagner *et al*, 2004). A Fisher's exact probability test showed that *FosB*(−/−) mice were significantly more prone to bleeding ($p = 0.023$) and self-injury ($p = 0.049$) compared to their (+/+) littermates after a single 10 mg/kg METH injection, suggesting that FosB deficiency increases the incidence of METH-induced self-injuries. All incidences of bleeding occurred within 2 h of the first METH injection. Further extension of injuries was not evident following the second METH injection. Moreover, even the mouse showing the largest lesion survived all four METH injections, and we observed significant healing of the lesion on the fourth day. Thus, it appeared that the METH-induced self-inflicted injuries were largely due to the first METH exposure, rather than being secondary to longer-term neurodegenerative changes.

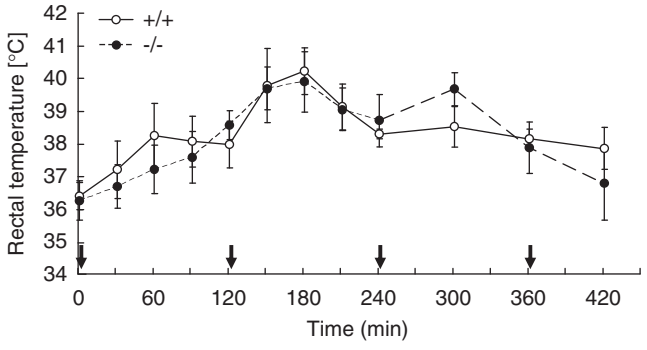

Figure 2 Effects of the *FosB* mutation on core body temperature during neurotoxic methamphetamine (METH) treatment. Rectal temperature of *FosB*(+/+) (open circle, $n = 5$) and of (−/−) (closed circle, $n = 5$) mice was measured during four injections of 10 mg/kg METH, indicated by arrows. Data are presented as mean ± SEM.

Altered Expression of *Sprouty* and *RGK* in *FosB*(−/−) Mice

We have previously shown that, during parental care, ERK induces *FosB*, and FosB then exerts its effect to induce *SPRY1* and *RAD*, both of which are negative feedback regulators for neuronal activation (Kuroda *et al*, 2007). We hypothesized that a similar molecular change might occur in some brain areas of *FosB*(−/−) mice on METH stimulation. Thus, we examined gene expression profiles in the frontoparietal cortex and striatum of *FosB*(+/+) and (−/−) mice after a single 10 mg/kg METH injection by qRT-PCR analyses. Preliminary time-course experiments showed that in the frontoparietal cortex of (+/+) mice both *SPRY1* and *RAD* induction were observed 2 h after METH injection (data not shown). Conversely, neither *SPRY1* nor *RAD* induction was observed in *FosB*(+/+) striatum. As mentioned in the Introduction, both *SPRY1* and *RAD* belong to a family of homologous genes, namely *Sprouty* and *RGK*, respectively. These homologous transcripts were examined together with *SPRY1* and *RAD* to determine if these family members were induced in the striatum instead.

A two-way ANOVA with the intersubject factors of genotype and treatment confirmed upregulation of immediately early genes (*c-Fos*, *FosB*, and *NGFI-B*) by METH treatment in both the frontoparietal cortex ($F_{1,20} = 16.78$, 27.42, and 68.60, respectively, $p < 0.001$ for all) and striatum

Table 1 Effects of the *FosB* Mutation on the Incidence of Bleeding and Skin Lesions 2 h After a 10 mg/kg METH Injection

		No bleeding	Bleeding of unknown origin	Bleeding with skin lesion	*N*
+/+	Saline	22 (100%)	0 (0%)	0 (0%)	22
	Methamphetamine	22 (96%)	0 (0%)	1 (4%)	23
−/−	Saline	22 (100%)	0 (0%)	0 (0%)	22
	Methamphetamine	16 (67%)	3 (13%)	5 (21%)	24

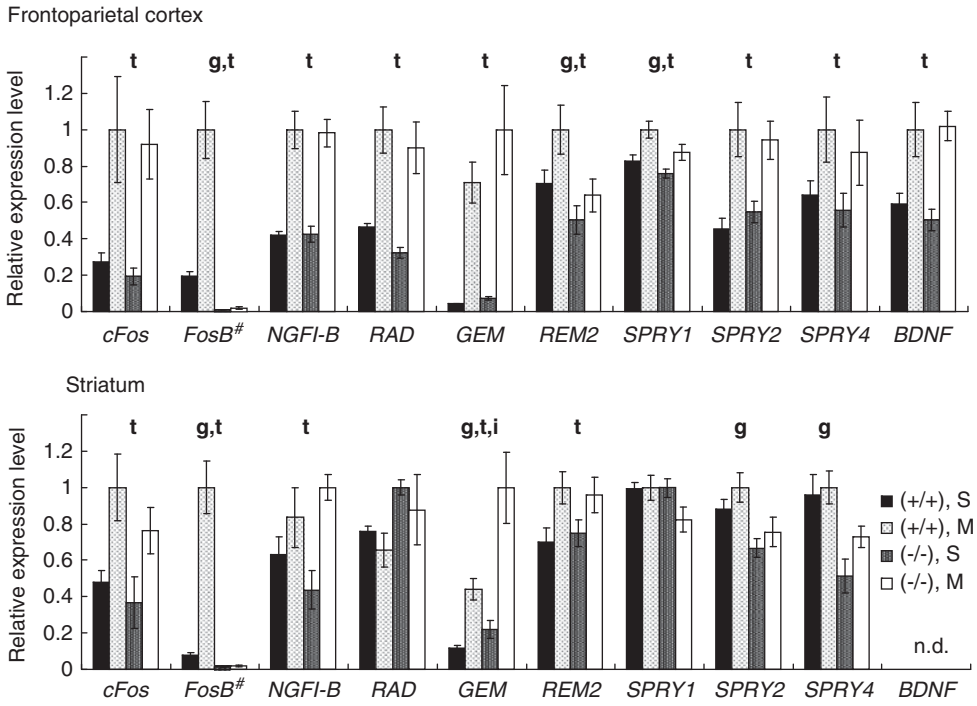

Figure 3 Effects of the *FosB* mutation on gene expression in the frontoparietal cortex and striatum 2 h after a single 10 mg/kg methamphetamine (METH) injection. Mean ± SEM relative gene expression levels in the frontoparietal cortex or in the striatum examined by qRT-PCR. *FosB*(+/+) and (−/−) mice were treated with either a single saline (S) or a 10 mg/kg METH (M) injection, and tissue was dissected 2 h after injection ($n = 6$ per group). Data are expressed as arbitrary units normalized to *GAPDH*, with highest values within a group set to 1. Letters above the bars indicate significant effects ($p < 0.05$) of genotype (g), treatment (t), and/or genotype–treatment interaction (i) by a two-way analysis of variance (ANOVA) with the intersubject factors of genotype and treatment. #genotype–treatment interaction was not statistically analyzed due to lack of *FosB* transcripts in *FosB*(−/−) mice; n.d., not reliably detected.

($F_{1,20} = 11.29$, 40.48, and 11.03; $p = 0.003$, < 0.001, and 0.003, respectively, Figure 3) as previously reported (Graybiel *et al*, 1990; Herdegen and Leah, 1998). Notably, in the frontoparietal cortex, all the *Sprouty* family genes ($F_{1,20} = 14.45$, 22.02, and 5.81; $p = 0.001$, < 0.001, and 0.026 for *SPRY1*, *2*, and *4*, respectively) and all *RGK* family genes tested ($F_{1,20} = 33.15$, 34.99, and 4.98; $p < 0.001$, < 0.001, and 0.037 for *RAD*, *GEM*, and *REM2*, respectively) were significantly induced by METH treatment. Brain-derived neurotrophic factor (*BDNF*) was also upregulated by METH treatment in the frontoparietal cortex ($F_{1,20} = 23.65$, $p < 0.001$; Figure 3), similar to previous reports for cocaine treatment (Le Foll *et al*, 2005). These findings were consistent with the previously suggested cellular functions of Sprouty and RGK proteins as negative feedback regulators of BDNF-RTK-ERK/calcium signaling during neuronal activation (Kelly, 2005; Kuroda *et al*, 2007; Mason *et al*, 2006). In the striatum, *GEM* ($F_{1,20} = 27.34$, $p < 0.001$) and *REM2* ($F_{1,20} = 9.15$, $p = 0.006$) were induced, but not *Sprouty* ($F_{1,20} = 3.66$, 2.28, and 2.04; $p = 0.07$, 0.14, and 0.17, for *SPRY1*, *2*, and *4*, respectively) by the METH treatment used. Expression of *BDNF* was about 1000 times lower than that in the frontoparietal cortex, and was too low to be reliably measured under our experimental conditions. This suggests that a different signaling mechanism exists in the frontoparietal cortex and in the striatum.

As expected, there was a clear absence of *FosB* expression in *FosB*(−/−) mice (significant genotype effects of $F_{1,20} = 50.98$, 51.73 for the frontoparietal cortex and striatum, respectively; $p < 0.001$; Figure 3), confirming ablation of the *FosB* gene. A two-way ANOVA showed significant genotype-dependent effects on *REM2* ($F_{1,20} = 8.30$, $p = 0.009$) and *SPRY1* ($F_{1,20} = 6.26$, $p = 0.02$) expression in the frontoparietal cortex, and on *GEM* ($F_{1,20} = 9.89$, $p = 0.005$), *SPRY2* ($F_{1,20} = 10.89$, $p = 0.004$), and *SPRY4* ($F_{1,20} = 15.43$, $p = 0.001$) in the striatum (Figure 3). A significant genotype–treatment interaction was found for *GEM* ($F_{1,20} = 9.89$, $p = 0.005$) in the striatum. Except for *GEM*, all of these changes showed a reduction in *Sprouty* and *RGK* genes, and no significant genotype–treatment interaction was found. Thus, FosB appears to regulate the basal expression of these genes. Unexpectedly, *GEM* induction was enhanced in *FosB*(−/−) mice compared with their (+/+) littermates (see Discussion). Taken together, these results suggest that many of Sprouty and RGK family members are induced by METH treatment in *FosB*(+/+) mice, and expression of *REM2* and *SPRY1* in the frontoparietal cortex and expression of *SPRY2* and *4* in the striatum depended at least partially on FosB.

Effect of the Null Mutation of *FosB* on Dopaminergic Terminal Degeneration After Neurotoxic METH Treatment

FosB has been implicated in drug addiction and regulation of the mesolimbic dopaminergic system (Nestler, 2001). For example, previous studies have shown that *FosB*(−/−) mice are hypersensitive to the psychomotor actions of cocaine (Hiroi *et al*, 1997). These previous reports suggest that the histological and behavioral METH hypersensitivity of *FosB*(−/−) mice could be due to the hypersensitivity of the dopaminergic system to psychostimulants in *FosB*(−/−)

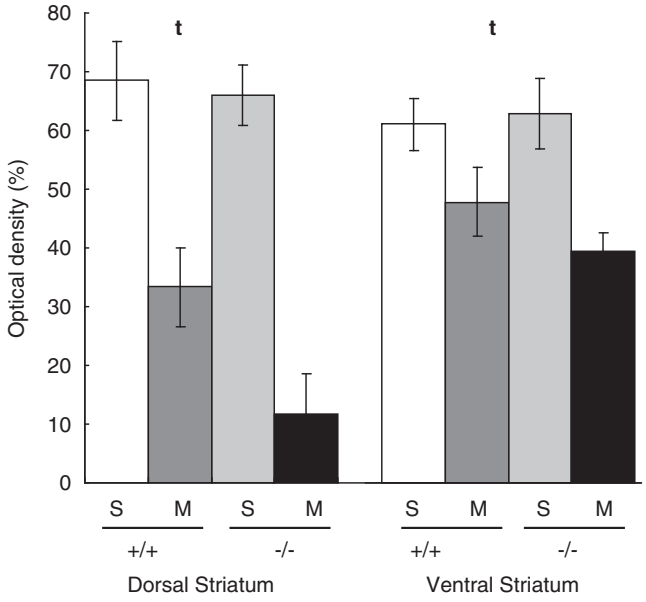

Figure 4 Effects of the *FosB* mutation on striatal tyrosine hydroxylase immunoreactivity in response to neurotoxic methamphetamine (METH) administration. Mean ± SEM optical density of tyrosine hydroxylase-immunopositive fibers in the dorsal and ventral striatum. *FosB*(+/+) and (−/−) mice ($n = 5$–6) were treated with four injections of saline (S) or 10 mg/kg METH (M) spaced 2 h apart and were examined for tyrosine hydroxylase immunoreactivity 3 days later. Further details are described in the Materials and methods section. Letters in charts indicate significant effects ($p < 0.05$) of treatment (t) by a two-way analysis of variance (ANOVA) with the intersubject factors of genotype and treatment.

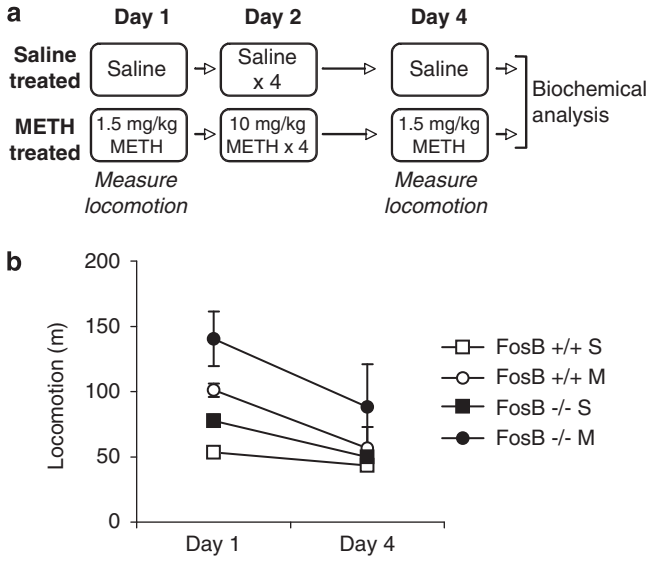

Figure 5 Effects of the null mutation of *FosB* on locomotor responses to methamphetamine (METH) following repeated treatment. (a) Summary of drug administration protocol used for locomotor and biochemical studies. (b) Horizontal locomotor activity during the 45 min period following 1.5 mg/kg METH administrations carried out on days 1 and 4. Data are presented as mean ± SEM; $n = 5$–6 per group. S, saline treated; M, METH treated. See Results section for statistical analysis.

mice. To test this, we first examined the density of tyrosine hydroxylase-immunopositive dopaminergic fibers in the dorsal (caudate putamen) and ventral striatum (nucleus accumbens) (Figure 4) using tissue obtained from the same mice as those studied for FJB staining in Figure 1, which had been treated with four 10 mg/kg administrations of METH at 2-h intervals. A two-way ANOVA with the intersubject factors of genotype and treatment confirmed significant decreases in tyrosine hydroxylase immunoreactivity following METH treatment in both the dorsal ($F_{1,18} = 47.53$, $p < 0.001$) and ventral striatum ($F_{1,18} = 13.69$, $p = 0.002$) as previously reported (McCann and Ricaurte, 2004). No significant effects of genotype, however, were found in either dorsal ($F_{1,18} = 3.41$, $p = 0.81$) or ventral striatum ($F_{1,18} = 0.44$, $p = 0.52$). Moreover, no significant genotype–treatment interactions were found either in dorsal ($F_{1,18} = 2.19$, $p = 0.157$) or ventral striatum ($F_{1,18} = 1.02$, $p = 0.326$). Dopaminergic terminals in *FosB*(−/−) striatum were therefore not found to be more vulnerable to METH-induced degeneration than those in *FosB*(+/+) littermates.

Effects of the Null Mutation of *FosB* on Locomotor Responses to METH After Repeated Treatment

To test the function of FosB in METH-induced locomotion and neurochemical responses simultaneously, we used the regimen of repeated METH administration detailed in Figure 5a. That is, *FosB*(−/−) and (+/+) mice were subjected to the same regimen of four injections of a high dose (10 mg/kg) of METH at 2-h intervals used in the histological and hyperthermia studies, but this was flanked temporally with two low-dose (1.5 mg/kg) administrations of METH used to assess the psychomotor properties of METH. For comparison, additional groups of mice were administered saline throughout. A two-way repeated-measures ANOVA showed a main effect of genotype ($F_{1,18} = 5.58$, $p = 0.030$), METH treatment ($F_{1,18} = 18.19$, $p < 0.001$), and time ($F_{1,18} = 10.61$, $p = 0.004$) on horizontal locomotion. There were no significant interactions between these factors. The main effects were due to an approximately 40% higher locomotor activity in *FosB*(−/−) mice, as has been previously reported (Hiroi *et al*, 1997). METH administration stimulated increases in locomotion in both genotypes during both measurements that were approximately equal compared to saline-treated control mice of the same genotype (Figure 5). There was a decrease in locomotor activity in all mice, regardless of treatment between the first (day 1) and second (day 4) locomotion measurements ($F_{1,18} = 10.609$, $p = 0.004$, no significant interactions with treatment or genotype). These results indicate that the null mutation of *FosB* causes a generally enhanced locomotor activity, but does not influence the psychomotor effects of METH at the 1.5 mg/kg dose administered in this study.

Effects of the Null Mutation of *FosB* on Biogenic Amines and Amino Acids

Immediately following the second locomotor measurement, animals were killed and brains were removed for neurochemical analysis. Tissues biopsies were taken from frozen sections of the frontoparietal cortex and the dorsal and ventral striatum, and analyzed by HPLC for biogenic amine dopamine, serotonin and their metabolites, and amino-acid content. For amino acids, we focused our analysis particularly on neuroactive compounds, such as those

Table 2 Summary of the Effect of the Null Mutation of *FosB* and METH Administration on Tissue Biochemical Content

Treatment	Saline		Methamphetamine		F score		
Genotype	***FosB*(+/+)**	***FosB*(−/−)**	***FosB*(+/+)**	***FosB*(−/−)**	**Genotype**	**Treatment**	**Interaction**
Frontoparietal cortex							
Dopamine	863 ± 291	644 ± 80	588 ± 47	591 ± 65	0.40	0.92	0.42
5-HT	2103 ± 169	1720 ± 99	1986 ± 67	1640 ± 81	9.50[a]	0.64	0.02
DOPAC	675 ± 76	737 ± 83	526 ± 58	531 ± 51	0.22	6.17[b]	0.16
HVA	0.16 ± 0.03	0.18 ± 0.02	0.16 ± 0.02	0.15 ± 0.01	0.02	0.47	0.82
5-HIAA	3143 ± 305	3534 ± 204	2832 ± 173	2759 ± 123	0.50	5.87[b]	1.08
3-MT	1506 ± 105	1595 ± 109	888 ± 78	909 ± 36	0.35	49.78[c]	0.14
Dopamine turnover	217 ± 40	199 ± 13	183 ± 10	151 ± 14	0.93	2.58	0.06
5-HT turnover	1.44 ± 0.24	1.92 ± 0.15	1.32 ± 0.09	1.57 ± 0.12	4.66[b]	1.97	0.45
Aspartate	2 002 101 ± 143 483	2 271 386 ± 117 185	2 057 045 ± 98 824	2 277 182 ± 131 161	3.75	0.06	0.04
Serine	519 244 ± 23 648	471 500 ± 23 081	566 901 ± 14 451	417 910 ± 12 192	23.80[c]	0.02	6.31[b]
Glycine	897 738 ± 49 512	791 071 ± 44 137	960 127 ± 52 530	964 342 ± 43 857	1.15	6.03[b]	1.33
Glutamate	10 822 461 ± 412 541	11 778 759 ± 688 003	11 898 097 ± 388 441	11 130 684 ± 286 375	0.04	0.19	3.04
Arginine	119 562 ± 8832	138 312 ± 13 715	122 813 ± 5723	111 627 ± 6652	0.17	1.30	2.36
Alanine	378 166 ± 19 089	434 195 ± 25 799	420 621 ± 13 531	385 787 ± 21 593	0.25	0.02	4.62[b]
Taurine	15 049 623 ± 972 040	16 882 232 ± 607 688	15 897 408 ± 590 618	16 609 734 ± 384 983	3.22	0.17	0.62
Tyrosine	71 428 ± 12 650	71 046 ± 7532	75 191 ± 10 976	68 664 ± 6715	0.14	0.00	0.10
GABA	3 283 089 ± 150 883	3 516 012 ± 106 266	3 232 211 ± 131 679	3 320 530 ± 109 647	1.57	0.93	0.32
Dorsal striatum							
Dopamine	108 253 ± 6140	95 862 ± 4079	2857 ± 321	4226 ± 2004	1.74	556.44[c]	2.71
5-HT	2768 ± 169	2451 ± 102	1753 ± 162	1462 ± 282	2.76	29.99[c]	0.01
DOPAC	18 865 ± 1206	18 489 ± 1327	2357 ± 274	2607 ± 790	0.00	233.29[c]	0.09
HVA	11 840 ± 515	10 597 ± 293	4624 ± 145	4179 ± 425	4.79[b]	312.98[c]	1.07
5-HIAA	1904 ± 124	1855 ± 60	2294 ± 76	2103 ± 242	0.76	5.37[b]	0.27
3-MT	8804 ± 557	8405 ± 148	1706 ± 205	1520 ± 475	0.55	313.22[c]	0.07
Dopamine turnover	0.25 ± 0.01	0.27 ± 0.01	2.16 ± 0.12	1.96 ± 0.31	0.36	143.87[c]	0.52
5-HT turnover	0.64 ± 0.04	0.70 ± 0.03	1.23 ± 0.08	1.49 ± 0.24	1.95	35.74[c]	0.72
Aspartate	2 210 649 ± 173 916	1 889 815 ± 85 922	2 301 472 ± 181 832	2 017 823 ± 190 934	3.56	0.47	0.01
Serine	622 122 ± 30 893	524 393 ± 6869	794 446 ± 26 922	565 626 ± 49 922	27.75[c]	11.80[a]	4.44[b]
Glycine	746 782 ± 16 438	620 909 ± 23 418	757 266 ± 33 710	699 745 ± 38 857	10.67[a]	2.55	1.47
Glutamate	10 615 960 ± 533 075	9 962 872 ± 347 905	10 876 150 ± 534 132	9 758 686 ± 1 024 985	1.98	0.00	0.14
Arginine	160 624 ± 8113	166 050 ± 8938	207 216 ± 9881	165 037 ± 17 686	2.57	4.14	4.48[b]
Alanine	264 040 ± 23 684	300 484 ± 10 927	359 199 ± 18 464	282 208 ± 29 546	0.92	3.24	7.02[b]
Taurine	20 113 313 ± 1 367 828	19 073 780 ± 469 117	21 804 666 ± 923 787	20 231 585 ± 1 637 668	1.26	1.49	0.05
Tyrosine	36 684 ± 12 916	28 200 ± 5647	79 152 ± 17 535	51 624 ± 7654	2.42	8.13[b]	0.68
GABA	1 946 677 ± 94 370	1 818 617 ± 58 006	1 939 780 ± 59 306	1 910 845 ± 129 597	0.78	0.23	0.31
Ventral striatum							
Dopamine	48 342 ± 5271	59 487 ± 2567	25 582 ± 1611	29 464 ± 1832	4.82[b]	59.46[c]	1.13
5-HT	3926 ± 345	3454 ± 135	3288 ± 409	2627 ± 291	3.45	5.77[b]	0.10
DOPAC	25 091 ± 2525	25 529 ± 4048	16 966 ± 2401	19 558 ± 2377	0.25	5.35[b]	0.13
HVA	10 936 ± 656	10 801 ± 777	7706 ± 518	7529 ± 507	0.06	24.99[c]	0.00
5-HIAA	3149 ± 205	2811 ± 133	3274 ± 233	2657 ± 177	6.38[b]	0.01	0.55
3-MT	5162 ± 582	6295 ± 250	3831 ± 160	3674 ± 329	1.59	26.08[c]	2.78
Dopamine turnover	0.71 ± 0.11	0.55 ± 0.08	0.88 ± 0.13	0.83 ± 0.09	1.13	5.00[b]	0.24
5-HT turnover	0.76 ± 0.05	0.76 ± 0.06	0.98 ± 0.13	0.96 ± 0.09	0.00	6.07[b]	0.02
Aspartate	2 005 782 ± 117 528	1 797 912 ± 74 523	2 175 627 ± 166 697	1 782 605 ± 137 759	5.84[b]	0.39	0.56
Serine	539 434 ± 46 591	496 727 ± 23 888	636 936 ± 61 195	446 196 ± 32 332	7.55[b]	0.31	3.04

Table 2 Continued

Treatment	Saline		Methamphetamine		F score		
Genotype	***FosB*(+/+)**	***FosB*(−/−)**	***FosB*(+/+)**	***FosB*(−/−)**	**Genotype**	**Treatment**	**Interaction**
Glycine	596 123 ± 30 185	527 264 ± 31 151	653 804 ± 32 171	556 878 ± 35 949	6.55[b]	1.80	0.19
Glutamate	8 912 187 ± 696 284	9 349 868 ± 573 593	9 736 331 ± 524 018	8 278 371 ± 532 718	0.72	0.04	2.48
Arginine	243 360 ± 16 296	230 803 ± 16 595	243 488 ± 9245	204 996 ± 12 474	3.15	0.77	0.81
Alanine	271 045 ± 18 687	313 618 ± 20 039	323 060 ± 30 974	270 852 ± 13 047	0.05	0.05	4.89[b]
Taurine	11 834 181 ± 899 756	13 123 554 ± 811 553	13 677 954 ± 980 646	12 404 658 ± 825 699	0.00	0.40	2.10
Tyrosine	116 397 ± 10 510	106 525 ± 9203	126 143 ± 12 153	106 244 ± 10 254	2.19	0.19	0.23
GABA	3 976 123 ± 253 153	3 058 752 ± 183 081	3 817 223 ± 248 443	3 437 538 ± 196 918	8.36[a]	0.24	1.44

DOPAC, dihydroxyphenylacetic acid; 5-HIAA, 5-hydroxyindoleacetic acid; HVA, homovanillic acid; 3-MT, 3-methoxytyramine; 5-HT, serotonin; GABA, γ-aminobutyric acid.

Analyses were carried out immediately following the final locomotor measurement detailed in Figure 5a. Values indicate pg/mg protein, except for turnover values, which are presented as ratios as described in the Materials and methods section. Note that there were no genotype- or treatment-dependent effects on tissue protein contents. Data are presented as mean ± SEM. $n = 5$–6 per group. Rightmost columns indicate the result of statistical analysis.

Degrees of freedom are 1, 18 in all cases except 3-MT in PFC, which are 1, 17 due to a single undetectable sample.

[a] $p < 0.01$.

[b] $p < 0.05$.

[c] $p < 0.001$.

acting at the glutamate (Glu) site of the *N*-methyl-D-aspartate (NMDA) receptor (glutamate and aspartate), at the co-agonist site of the NMDA receptor (glycine), GABA, and arginine, as it is a precursor for nitric oxide synthesis (Sakurai *et al*, 2004). We also included several amino acids with either putative or unspecified neuroactivity, such as taurine, alanine, and serine. The quantification of amino acids was performed by comparing it to a standard cocktail of L-type amino acids (see Materials and methods for details). The results of the analysis are shown in Table 2 alongside the results of the statistical analyses. Overall, the most pervasive genotype-dependent difference observed was reduced tissue serine content in *FosB*(−/−) mice (Figure 6). A two-way ANOVA with the intersubject factors of genotype and treatment showed significant effects of genotype in the serine content in the frontoparietal cortex ($F_{1,18} = 23.80$, $p < 0.001$), dorsal striatum ($F_{1,18} = 27.75$, $p < 0.001$), and ventral striatum ($F_{1,18} = 7.55$, $p = 0.013$). Serine content was consistently lower (approximately 80–90% of the amount of *FosB*(+/+) mice in saline-treated groups, and approximately 70% in METH-treated groups) in all brain areas of *FosB*(−/−) mice. A significant effect of treatment was found in the dorsal striatum ($F_{1,18} = 11.80$, $p = 0.003$), and significant genotype–treatment interactions were found in the frontoparietal cortex ($F_{1,18} = 6.31$, $p = 0.022$) and dorsal striatum ($F_{1,18} = 4.44$, $p = 0.049$) (Figure 6). *FosB*(−/−) mice therefore had lower basal serine levels that did not increase after METH administration. There was a differential effect of METH administration on tissue alanine content between *FosB*(−/−) and (+/+) mice (Figure 6). Although there were no significant effects of genotype or treatment in any brain region, significant interactions between genotype and treatment were found in all brain regions ($F_{1,18} = 4.62$, $p = 0.045$ in the frontoparietal cortex; $F_{1,18} = 7.02$, $p = 0.016$ in dorsal striatum; and $F_{1,18} = 4.89$, $p = 0.040$ in ventral striatum). Whereas METH treatment stimulated mild increases in alanine content in *FosB*(+/+) mice, there was either no change or a decrease in *FosB*(−/−) mice. Notably, glycine was significantly lower in both the dorsal ($F_{1,18} = 10.67$, $p = 0.0043$) and the ventral striatum ($F_{1,18} = 6.55$, $p = 0.0197$) of *FosB*(−/−) mice (Figure 6).

There were several other significant effects of genotype, such as serotonin content in the frontoparietal cortex and GABA content in the ventral striatum (Table 2). All of these changes were due to lower tissue contents in *FosB*(−/−) compared with their (+/+) littermates. It should be noted, however, that no significant effect of genotype or genotype–treatment interaction was found in dopamine or dihydroxyphenylacetic acid (DOPAC) content or in dopamine turnover throughout this analysis, except dopamine content was mildly higher in the ventral striatum of *FosB*(−/−) mice ($F_{1,18} = 4.82$, $p = 0.042$). METH treatment induced significant reductions in dopamine and DOPAC content in the ventral and especially the dorsal striatum, as previously reported (Cadet *et al*, 2003), verifying our experimental procedures.

It is important to note that we did not apply any correction for the multiple comparisons made in the biochemical data presented here, as others have suggested that this may lead one to overlook informative findings (see Curran-Everett, 2000; Perneger, 1998 for discussion). The results, however, should be viewed in this context.

Effect of the Null Mutation of *FosB* on the BBB Dysfunction After Neurotoxic METH Treatment

Methamphetamine-induced BBB dysfunction has been suggested as a mean by which METH induces neurotoxicity (Dietrich, 2009). Loss of BBB integrity allows penetration of blood-born macromolecules, such as IgG and albumin, into perivascular tissue (extravasation). IgG extravasation can be detected by IgG immunostaining on brain tissue, even after transcardial perfusion. To assess if *FosB*(−/−) mice are especially vulnerable to METH-induced BBB damage, we performed IgG immunohistochemistry on brain sections from mice treated with four 10 mg/kg METH administrations. The numbers of discrete IgG-immunoreactive bodies

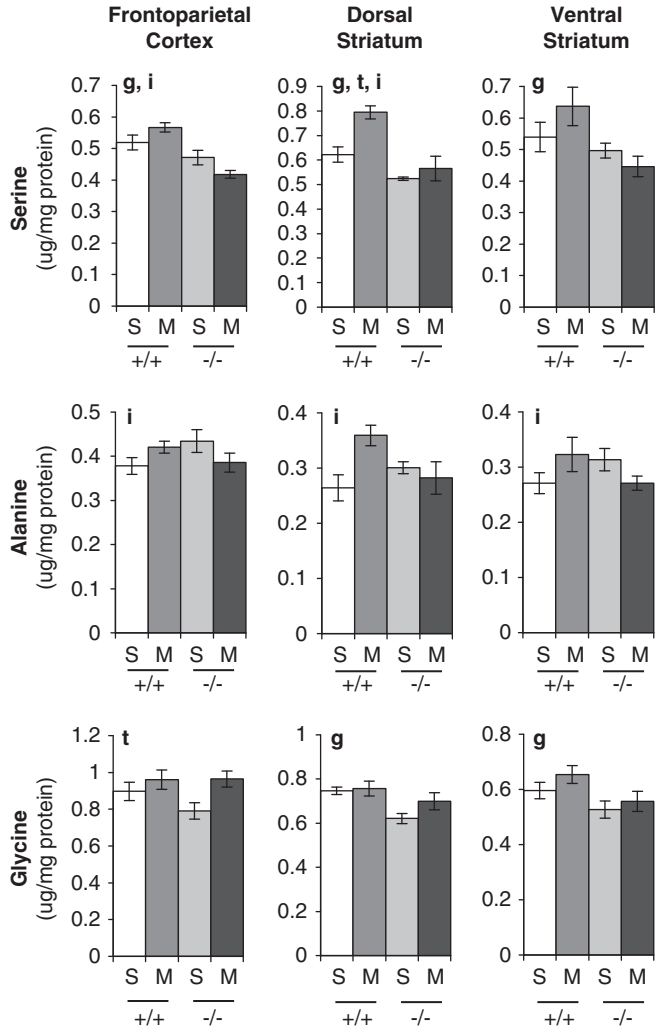

Figure 6 Graphical representation of the effect of the null mutation of *FosB* on basal and methamphetamine (METH)-induced changes in tissue serine, alanine and glycine content. Analyses were carried out immediately after the final locomotor measurement detailed in Figure 5a. S, saline treated; M, METH treated. Data are presented as mean ± SEM; $n = 5$–6 per group. Letters above the bars indicate significant effects ($p < 0.05$) of genotype (g), treatment (t), and/or genotype–treatment interaction (i) by a two-way analysis of variance (ANOVA) with the intersubject factors of genotype and treatment.

were quantified and analyzed by a two-way ANOVA with the intersubject factors of genotype and treatment (Figure 7c). Significant effects of treatment were found in the frontoparietal cortex ($F_{1,18} = 66.46$, $p < 0.001$), striatum ($F_{1,18} = 34.75$, $p < 0.001$), and piriform cortex ($F_{1,18} = 12.40$, $p = 0.002$). We detected significant METH-induced IgG extravasation in the striatum, frontoparietal cortex, and in the piriform cortex of both *FosB*(+/+) and (−/−) mice (Figure 7a and b), indicative of a particularly vulnerable BBB in these brain regions. It is notable that these brain areas are the same areas that exhibited FJB-positive cells (Figure 1). Especially, in the parietal cortex, IgG extravasation and FJB-positive neurons were confined to both layer III and superficial layer IV in the somatosensory cortex, area 1. Significant effects of genotype were found in the frontoparietal cortex ($F_{1,18} = 20.25$, $p = 0.001$) and in the piriform cortex ($F_{1,18} = 6.27$, $p = 0.021$), but not in the striatum ($F_{1,18} = 1.43$, $p = 0.246$). Significant genotype–treatment interactions were found in the frontoparietal cortex ($F_{1,18} = 19.19$, $p < 0.001$) and piriform cortex ($F_{1,18} = 6.86$, $p = 0.016$), but not in the striatum ($F_{1,18} = 1.60$, $p = 0.220$). That is, after METH treatment, the frontoparietal and piriform cortices of *FosB*(−/−) mice contained significantly more IgG-immunoreactive bodies than those of their (+/+) littermates.

DISCUSSION

Role of *Fos* Family Genes in Neuroprotection Against METH

Methamphetamine neurotoxicity produces two major end results: monoaminergic terminal degeneration and postsynaptic, non-monoaminergic neuronal death. The latter can be due to apoptosis or necrosis (Gold *et al*, 2009). In this study, we showed that *FosB*(−/−) mice are more vulnerable to a neurotoxic regimen of METH administration by showing an increased FJB-positive degenerated neurons in the frontoparietal cortex and striatum. We found no evidence of exaggerated monoaminergic terminal degeneration (using tyrosine hydroxylase immunoreactivity or tissue monoamine contents) or of apoptosis (using TUNEL and caspase-3 staining) in METH-treated *FosB* (−/−) brains compared with their (+/+) littermates. Thus, our data suggest that FosB is more important for neuroprotection against nonapoptotic cell death in postsynaptic neurons, at least in the frontoparietal cortex and striatum. These findings contrast with c-*Fos*(−/−) and (+/−) mice, which show exacerbated striatal dopaminergic terminal loss and dopamine-reuptake sites, and more neuronal apoptosis in their cortices and striata (Deng *et al*, 1999). Thus, although both c-Fos and FosB are neuroprotective against METH-induced toxicity, their mechanisms of action appear to be distinct.

Mechanisms of FosB-Mediated Protection of Postsynaptic Neurons

Multiple mechanisms, including hyperthermia, mitochondrial stress and subsequent apoptosis, and BBB dysfunction, have been implicated in METH-induced neuronal death (Krasnova and Cadet, 2009). Among these, we attempted to dissect the relevant mechanisms by which FosB modulates responses to METH. We found that METH-induced hyperthermia was not exacerbated in *FosB*(−/−) mice. In contrast, we found that BBB dysfunction, visualized by IgG extravasation, was intensified in the cortices of *FosB*(−/−) mice. Moreover, the localities of IgG immunoreactive bodies were highly coincident with FJB-positive degenerating neurons, especially in the parietal cortex. Specifically, both FJB-positive cells and IgG-immunoreactive bodies were restricted to deep layer III and superficial layer IV of the parietal cortex, area 1. In addition, in the striatum of adjacent serial sections from the same mice, the distribution patterns of degenerating neurons and IgG immunoreactive bodies were very similar. These patterns, however, were not consistent with the ablation pattern of tyrosine hydroxylase immunoreactivity (data not shown). A previous report shows that the striatal subregion that contains the greatest

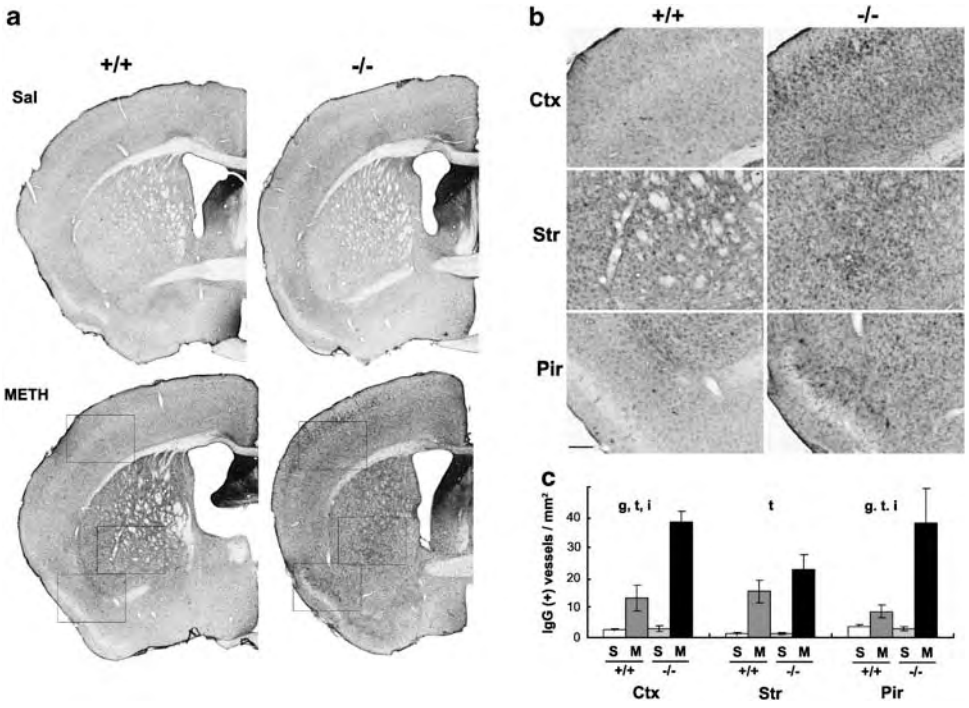

Figure 7 Effects of the *FosB* mutation on IgG extravasation after neurotoxic methamphetamine (METH) administration. *FosB*(+/+) and (−/−) mice were treated with four injections of saline (S, $n=5$ each) or 10 mg/kg METH (M, $n=6$ each), and were examined for IgG leakage through the blood–brain barrier 3 days later by IgG immunostaining (a). (b) High magnification images of the rectangular fields illustrated in (a), from top to bottom, the frontoparietal cortex (Ctx), striatum (Str), and the piriform cortex (Pir) of METH-treated *FosB*(+/+) and (−/−) mice, respectively. Scale bar = 200 μm. (c) Mean ± SEM counts of IgG immunoreactive bodies. Letters above the bars indicate significant effects ($p<0.05$) of genotype (g), treatment (t), and/or genotype–treatment interaction (i) by a two-way analysis of variance (ANOVA) with the intersubject factors of genotype and treatment.

numbers of degenerated neurons and axons is different from the subregion showing the greatest loss of tyrosine hydroxylase immunoreactivity (Bowyer *et al*, 2008). These findings suggest that the mechanism of dopamine terminal damage is distinct from the mechanism mediating postsynaptic neuronal death within the striatum. Of note, independent mechanisms of striatal dopamine terminal damage from that of parietal cortical cell injury have been reported. That is, animals pretreated with a dopamine transport inhibitor before METH show parietal cortical cell body injury; however, they do not show loss in striatal tyrosine hydroxylase immunoreactivity (Eisch *et al*, 1998). In this study, we found that the genetic inactivation of *FosB* causes the opposite effects from pharmacological inhibition of the dopamine transporter, ie, it does not enhance the loss of tyrosine hydroxylase immunoreactivity, but enhances parietal cortical cell injuries. FosB, therefore, might not be critically involved in the dopamine transporter-mediated METH action on dopaminergic terminals.

FosB, Amino-Acid Metabolism, and Astroglial Function

We found a decrease and/or attenuated induction of the small neutral amino acids, serine, alanine, and glycine after METH treatment in most of the *FosB*(−/−) forebrain areas analyzed. Although the amino-acid measurements in this study were not designed to distinguish the two stereoisomers of L- and D-amino acids, most of the serine detected in this study is presumably the L-stereoisomer, as this constitutes the majority found in higher animals (Furuya and Watanabe, 2003). L-Serine is an important precursor of D-serine. D-Serine and glycine are both potent co-agonists for NMDA-type glutamate receptors (Mothet *et al*, 2000). Moreover, L-serine and L-alanine themselves exert their effect as neurotrophic compounds, as they support the survival of neurons under serum- and glia-free culture conditions (Furuya *et al*, 2000). Altered regulation of these small amino acids in the forebrains of *FosB*(−/−) mice may therefore partly mediate the increased vulnerability of postsynaptic neurons after a neurotoxic dose of METH. This finding may also be relevant to the previous reports showing that *FosB*(−/−) mice have decreased tolerance to repeated electroconvulsive seizures and reduced NMDA receptor upregulation in the superficial layers of the neocortex (Hiroi *et al*, 1998). Specific investigation of D-serine content and NMDA receptor function in *FosB*(−/−) mutant mice could be an intriguing avenue for future studies.

L-Serine is produced mainly in astrocytes rather than in neurons (Furuya and Watanabe, 2003; Verleysdonk and Hamprecht, 2000). Thus, astroglial dysfunction is likely the cause of lower serine levels in the forebrain regions of *FosB*(−/−) mice. This notion is supported by our previous finding that astrocytes in the forebrains of *FosB*(−/−) mice exhibited persistent upregulation of glial fibrillary acidic protein under basal conditions (Kuroda *et al*, 2008). Relevant to this topic, we found here that *FosB*(−/−) frontoparietal and piriform cortices show enhanced METH-induced BBB dysfunction. Astrocytes, whose endfeet encircle neural capillaries, form the BBB together with vascular endothelial cells (Dietrich, 2009). As we found that neuronal death was colocalized with BBB dysfunction,

astroglial dysfunction may mediate the enhanced METH toxicity in the forebrains of *FosB*(−/−) mice. Indeed, several studies have reported the relevance of BBB dysfunction with neuronal death (Bowyer and Ali, 2006a; Kiyatkin *et al*, 2007). In the case of the excitotoxic injury model made by hippocampal kinate injection, however, neuronal death and BBB breakdown are separate, independent processes: BBB dysfunction occurs too late to initiate neurodegeneration, and BBB breakdown occurs without neuronal death (Chen *et al*, 1999). The causal relationship of these multiple events remains to be clarified.

Another puzzling fact is that FosB expression is confined primarily in neurons, as FosB expression in glial cells tends to be undetectable, even under stimulation (Herdegen and Leah, 1998). The FosB protein in neurons may therefore cause wide arrays of abnormalities in astrocyte metabolism through neuron–glia communication. *FosB*(−/−) mice might be an interesting model system for understanding the cross talk between neurons and glia cells.

FosB-Mediated Intracellular Signaling Regulation in Response to Neurotoxic Doses of METH

After psychostimulant administration, elevation of intracellular calcium levels and ERK phosphorylation occurs in many brain areas, resulting in the induction of Fos family transcription factors (Hope *et al*, 1994; Valjent *et al*, 2004). Our previous study shows that the null mutation of *FosB* attenuates upregulation of *SPRY1* and *RAD*, negative feedback regulators of ERK and calcium signaling, respectively, in the medial preoptic area (Kuroda *et al*, 2007). Here we found that basal and stimulated expression of *Sprouty* and *RGK* genes tended to be lower in *FosB*(−/−) mice, with the only exception of higher *GEM* expression in the striatum of *FosB*(−/−) mice. As mentioned in the Introduction, METH-induced *GEM* upregulation is dependent on c-Fos (Cadet *et al*, 2002). Therefore *GEM* induction could be overly compensated by c-Fos in the striatum of *FosB*(−/−) mice. Sprouty is a major class of ligand-inducible inhibitors of RTK/ERK signaling pathway (Mason *et al*, 2006), and RGK is a potent inhibitor of calcium overinflux into activated cells (Kelly, 2005). Reduced expression of Sprouty and RGK can cause the overactivation of neurons, in terms of ERK phosphorylation and intracellular calcium elevation, respectively. Of note, it has been reported that the L-type calcium channel agonist BayK8644 can cause self-injurious biting (Jinnah *et al*, 1999). RGK proteins are known to downregulate calcium influx by sequestering L-type calcium channels (Kelly, 2005). These observations by no means prove our hypothesis that the ERK/calcium–Fos–Sprouty/RGK molecular cascade could exert its effect as a negative feedback loop against METH-induced neurotoxicity, but at least are in accord. Fos target genes involved in such a general negative feedback might be found more easily than Fos target genes that have more specific functions in certain neuronal types. Indeed, all previous studies that have detected attenuated RGK induction in *Fos*-gene-targeted mice (Cadet *et al*, 2002; Kuroda *et al*, 2007; Salzmann *et al*, 2006) used grossly dissected brain tissue, containing different neuronal populations.

In summary, the current study suggests two possible mechanisms of FosB-mediated neuroprotection: one is through induction of negative feedback regulation within postsynaptic neurons through *Sprouty* and *RGK*. Another is supporting astroglial function such as maintenance of the BBB, and metabolism of serine and glycine, which are important glial modulators of nerve cells. These two mechanisms are not necessarily mutually exclusive, and the former may cause the latter through the neuron–glia interaction. It is important to recognize, however, that ultimately the diverse findings provided here are correlative, and more directed study is necessary to provide a causative relationship.

ACKNOWLEDGEMENTS

We thank Yoshio Hirabayashi for helpful discussion, Tetsuaki Ara and Taeko Nemoto for technical assistance, and the RIKEN Research Resource Center for maintenance of animals. This research was supported by RIKEN, Grants-in-Aid for Scientific Research from the Ministry of Education, Culture, Sports, Science, and Technology, Japan (2006–2008 to KOK and KT) and by the Uehara Memorial Foundation (2009 to KOK).

DISCLOSURE

The authors declare no conflict of interest.

REFERENCES

Berghorn KA, Bonnett JH, Hoffman GE (1994). cFos immunoreactivity is enhanced with biotin amplification. *J Histochem Cytochem* **42**: 1635–1642.

Bowyer JF (1995). The role of hyperthermia in amphetamine's interactions with NMDA receptors, nitric oxide, and age to produce neurotoxicity. *Ann NY Acad Sci* **765**: 309–310.

Bowyer JF, Ali S (2006a). High doses of methamphetamine that cause disruption of the blood–brain barrier in limbic regions produce extensive neuronal degeneration in mouse hippocampus. *Synapse* **60**: 521–532.

Bowyer JF, Robinson B, Ali S, Schmued LC (2008). Neurotoxic-related changes in tyrosine hydroxylase, microglia, myelin, and the blood–brain barrier in the caudate–putamen from acute methamphetamine exposure. *Synapse* **62**: 193–204.

Bowyer JF, Schmued LC (2006b). Fluoro-Ruby labeling prior to an amphetamine neurotoxic insult shows a definitive massive loss of dopaminergic terminals and axons in the caudate–putamen. *Brain Res* **1075**: 236–239.

Brown JR, Ye H, Bronson RT, Dikkes P, Greenberg ME (1996). A defect in nurturing in mice lacking the immediate early gene *fosB*. *Cell* **86**: 297–309.

Cadet JL, Jayanthi S, Deng X (2003). Speed kills: cellular and molecular bases of methamphetamine-induced nerve terminal degeneration and neuronal apoptosis. *FASEB J* **17**: 1775–1788.

Cadet JL, McCoy MT, Ladenheim B (2002). Distinct gene expression signatures in the striata of wild-type and heterozygous c-fos knockout mice following methamphetamine administration: evidence from cDNA array analyses. *Synapse* **44**: 211–226.

Chen ZL, Indyk JA, Bugge TH, Kombrinck KW, Degen JL, Strickland S (1999). Neuronal death and blood–brain barrier breakdown after excitotoxic injury are independent processes. *J Neurosci* **19**: 9813–9820.

Curran-Everett D (2000). Multiple comparisons: philosophies and illustrations. *Am J Physiol Regul Integr Comp Physiol* **279**: R1–R8.

Davidson C, Gow AJ, Lee TH, Ellinwood EH (2001). Methamphetamine neurotoxicity: necrotic and apoptotic mechanisms and relevance to human abuse and treatment. *Brain Res Brain Res Rev* **36**: 1–22.

Deng X, Ladenheim B, Tsao LI, Cadet JL (1999). Null mutation of c-fos causes exacerbation of methamphetamine-induced neurotoxicity. *J Neurosci* **19**: 10107–10115.

Deng X, Wang Y, Chou J, Cadet JL (2001). Methamphetamine causes widespread apoptosis in the mouse brain: evidence from using an improved TUNEL histochemical method. *Brain Res Mol Brain Res* **93**: 64–69.

Dietrich JB (2009). Alteration of blood–brain barrier function by methamphetamine and cocaine. *Cell Tissue Res* **336**: 385–392.

Eisch AJ, Schmued LC, Marshall JF (1998). Characterizing cortical neuron injury with Fluoro-Jade labeling after a neurotoxic regimen of methamphetamine. *Synapse* **30**: 329–333.

Franklin KBJ, Paxinos G (2007). *The Mouse Brain in Stereotaxic Coordinates* 3rd edn. Academic Press: San Diego. pp 360.

Furuya S, Tabata T, Mitoma J, Yamada K, Yamasaki M, Makino A *et al* (2000). -Serine and glycine serve as major astroglia-derived trophic factors for cerebellar Purkinje neurons. *Proc Natl Acad Sci USA* **97**: 11528–11533.

Furuya S, Watanabe M (2003). Novel neuroglial and glioglial relationships mediated by L-serine metabolism. *Arch Histol Cytol* **66**: 109–121.

Glowinski J, Iversen LL (1966). Regional studies of catecholamines in the rat brain. I. The disposition of [3H]norepinephrine, [3H]dopamine and [3H]dopa in various regions of the brain. *J Neurochem* **13**: 655–669.

Gold MS, Kobeissy FH, Wang KK, Merlo LJ, Bruijnzeel AW, Krasnova IN *et al* (2009). Methamphetamine- and trauma-induced brain injuries: comparative cellular and molecular neurobiological substrates. *Biol Psychiatry* **66**: 118–127.

Gown AM, Willingham MC (2002). Improved detection of apoptotic cells in archival paraffin sections: immunohistochemistry using antibodies to cleaved caspase 3. *J Histochem Cytochem* **50**: 449–454.

Graybiel AM, Moratalla R, Robertson HA (1990). Amphetamine and cocaine induce drug-specific activation of the *c-fos* gene in striosome-matrix compartments and limbic subdivisions of the striatum. *Proc Natl Acad Sci USA* **87**: 6912–6916.

Herdegen T, Leah JD (1998). Inducible and constitutive transcription factors in the mammalian nervous system: control of gene expression by Jun, Fos and Krox, and CREB/ATF proteins. *Brain Res Brain Res Rev* **28**: 370–490.

Hiroi N, Brown JR, Haile CN, Ye H, Greenberg ME, Nestler EJ (1997). FosB mutant mice: loss of chronic cocaine induction of Fos-related proteins and heightened sensitivity to cocaine's psychomotor and rewarding effects. *Proc Natl Acad Sci USA* **94**: 10397–10402.

Hiroi N, Marek GJ, Brown JR, Ye H, Saudou F, Vaidya VA *et al* (1998). Essential role of the FosB gene in molecular, cellular, and behavioral actions of chronic electroconvulsive seizures. *J Neurosci* **18**: 6952–6962.

Hope BT, Nye HE, Kelz MB, Self DW, Iadarola MJ, Nakabeppu Y *et al* (1994). Induction of a long-lasting AP-1 complex composed of altered Fos-like proteins in brain by chronic cocaine and other chronic treatments. *Neuron* **13**: 1235–1244.

Jinnah HA, Yitta S, Drew T, Kim BS, Visser JE, Rothstein JD (1999). Calcium channel activation and self-biting in mice. *Proc Natl Acad Sci USA* **96**: 15228–15232.

Katayama K, Yamada K, Ornthanalai VG, Inoue T, Ota M, Murphy NP *et al* (2008). Slitrk1-deficient mice display elevated anxiety-like behavior and noradrenergic abnormalities. *Mol Psychiatry* (E-pub ahead of print).

Kelly K (2005). The RGK family: a regulatory tail of small GTP-binding proteins. *Trends Cell Biol* **15**: 640–643.

Kita T, Wagner GC, Nakashima T (2003). Current research on methamphetamine-induced neurotoxicity: animal models of monoamine disruption. *J Pharmacol Sci* **92**: 178–195.

Kiyatkin EA, Brown PL, Sharma HS (2007). Brain edema and breakdown of the blood–brain barrier during methamphetamine intoxication: critical role of brain hyperthermia. *Eur J Neurosci* **26**: 1242–1253.

Krasnova IN, Cadet JL (2009). Methamphetamine toxicity and messengers of death. *Brain Res Rev* **60**: 379–407.

Kuroda KO, Meaney MJ, Uetani N, Fortin Y, Ponton A, Kato T (2007). ERK-FosB signaling in dorsal MPOA neurons plays a major role in the initiation of parental behavior in mice. *Mol Cel Neurosci* **36**: 121–131.

Kuroda KO, Meaney MJ, Uetani N, Kato T (2008). Neurobehavioral basis of the impaired nurturing in mice lacking the immediate early gene *FosB*. *Brain Res* **1211**: 57–71.

Le Foll B, Diaz J, Sokoloff P (2005). A single cocaine exposure increases BDNF and D3 receptor expression: implications for drug-conditioning. *NeuroReport* **16**: 175–178.

Mason JM, Morrison DJ, Basson MA, Licht JD (2006). Sprouty proteins: multifaceted negative-feedback regulators of receptor tyrosine kinase signaling. *Trends Cell Biol* **16**: 45–54.

McCann UD, Ricaurte GA (2004). Amphetamine neurotoxicity: accomplishments and remaining challenges. *Neurosci Biobehav Rev* **27**: 821–826.

Mothet JP, Parent AT, Wolosker H, Brady Jr RO, Linden DJ, Ferris CD *et al* (2000). -Serine is an endogenous ligand for the glycine site of the *N*-methyl-D-aspartate receptor. *Proc Natl Acad Sci USA* **97**: 4926–4931.

Nestler EJ (2001). Molecular basis of long-term plasticity underlying addiction. *Nat Rev Neurosci* **2**: 119–128.

Numan M, Numan MJ, Marzella SR, Palumbo A (1998). Expression of c-fos, fos B, and egr-1 in the medial preoptic area and bed nucleus of the stria terminalis during maternal behavior in rats. *Brain Res* **792**: 348–352.

Perneger TV (1998). What's wrong with Bonferroni adjustments. *BMJ* **316**: 1236–1238.

Ryan LJ, Linder JC, Martone ME, Groves PM (1990). Histological and ultrastructural evidence that D-amphetamine causes degeneration in neostriatum and frontal cortex of rats. *Brain Res* **518**: 67–77.

Sakurai S, Ishii S, Umino A, Shimazu D, Yamamoto N, Nishikawa T (2004). Effects of psychotomimetic and antipsychotic agents on neocortical and striatal concentrations of various amino acids in the rat. *J Neurochem* **90**: 1378–1388.

Salzmann J, Canestrelli C, Noble F, Marie-Claire C (2006). Analysis of transcriptional responses in the mouse dorsal striatum following acute 3,4-methylenedioxymethamphetamine (ecstasy): identification of extracellular signal-regulated kinase-controlled genes. *Neuroscience* **137**: 473–482.

Schmued LC, Bowyer JF (1997). Methamphetamine exposure can produce neuronal degeneration in mouse hippocampal remnants. *Brain Res* **759**: 135–140.

Schmued LC, Hopkins KJ (2000). Fluoro-Jade B: a high affinity fluorescent marker for the localization of neuronal degeneration. *Brain Res* **874**: 123–130.

Sulzer D, Sonders MS, Poulsen NW, Galli A (2005). Mechanisms of neurotransmitter release by amphetamines: a review. *Prog Neurobiol* **75**: 406–433.

Tata DA, Yamamoto BK (2007). Interactions between methamphetamine and environmental stress: role of oxidative stress, glutamate and mitochondrial dysfunction. *Addiction* **102**(Suppl 1): 49–60.

Valjent E, Pages C, Herve D, Girault JA, Caboche J (2004). Addictive and non-addictive drugs induce distinct and specific patterns of ERK activation in mouse brain. *Eur J Neurosci* **19**: 1826–1836.

Verleysdonk S, Hamprecht B (2000). Synthesis and release of L-serine by rat astroglia-rich primary cultures. *Glia* **30**: 19–26.

Wagner GC, Avena N, Kita T, Nakashima T, Fisher H, Halladay AK (2004). Risperidone reduction of amphetamine-induced self-injurious behavior in mice. *Neuropharmacology* **46**: 700–708.